ORIGINAL PAPER

Up-Conversion Luminescence of the NaRF$_4$-NaR′F$_4$ (R: Y, Yb, Er) Core-Shell Nanomaterials

Iko Hyppänen · Jorma Hölsä · Jouko Kankare ·
Mika Lastusaari · Laura Pihlgren · Tero Soukka

Abstract Up-converting NaRF$_4$-NaR′F$_4$ (R: Y, Yb, Er) nanomaterials with different core-shell combinations were prepared with the co-precipitation method. The X-ray powder diffraction (XPD) measurements revealed the presence of both the cubic and hexagonal NaRF$_4$ phases. The crystallite sizes calculated with the Scherrer formula were 100 and 150 nm for the cubic and hexagonal phases, respectively. The FT-IR spectra showed water impurities. The up-conversion luminescence and luminescence decays were studied with NIR laser excitation at 970 nm. The up-conversion luminescence spectra showed strong red (640–685 nm) ($^4F_{9/2} \rightarrow {}^4I_{15/2}$) and moderate green (515–560 nm) ($^2H_{11/2}$, $^4S_{3/2} \rightarrow {}^4I_{15/2}$) Er^{3+} luminescence. The strongest up-conversion luminescence and longest red luminescence decay was obtained from the Na(Y,Yb)F$_4$-NaErF$_4$ core-shell combination.

Keywords Sodium yttrium tetrafluoride · Ytterbium · Erbium · Core-shell · Nanocrystals · Up-conversion luminescence

I. Hyppänen · J. Hölsä · J. Kankare · M. Lastusaari ·
L. Pihlgren (✉)
Department of Chemistry, University of Turku,
FI-20014 Turku, Finland
e-mail: laerle@utu.fi

I. Hyppänen
Graduate School of Chemical Sensors and Microanalytical
Systems (CHEMSEM),
Espoo, Finland

J. Hölsä · J. Kankare · M. Lastusaari
Turku University Centre for Materials and Surfaces (MatSurf),
Turku, Finland

L. Pihlgren
Graduate School of Materials Research (GSMR),
Turku, Finland

T. Soukka
Department of Biotechnology, University of Turku,
FI-20520 Turku, Finland

Introduction

Photon up-conversion is a unique type of luminescence in which low-energy radiation (NIR) is converted to higher-energy radiation [1, 2] using certain combinations of a sensitizer (*e.g.* Yb, Er and Sm) and an activator (*e.g.* Er, Ho, Pr and Tm). Recently the core-shell structures (layer materials where the shell is grown on the surface of the core) have been reported to improve the up-conversion efficiency by enhancing the energy transfer from the sensitizer to the activator [3–5]. Core-shell compositions have been employed for different functions widely [6–12]. The shell (*e.g.* silica) may act as a protective coating around a sensitive core or as a layer preventing particle aggregation [6, 7]. Silica shells have also been used to facilitate the binding of biomolecules on the nanoparticles [8]. Inactive core materials (*e.g.* polystyrene) have been covered with a luminescent shell [9]. The syntheses of core-shell structured luminescent nanoparticles by using passive inorganic shells (*e.g.* non-doped LaPO$_4$, LaF$_3$ and NaYF$_4$) to cover similar rare earth doped cores have been reported [10–12]. Materials with structures and unit cell dimensions similar to those of the rare earth doped cores have been chosen as the shells to avoid the formation of distortions at the core-shell interfaces. Since the research of the different combinations of the efficiently up-converting NaRF$_4$-NaR′F$_4$

core-shell nanomaterials is omitted in the literature, systematic study of these materials is required.

In this work, five different $NaRF_4$-$NaR'F_4$ (R: Y, Yb, Er) core-shell nanomaterial combinations, $NaYF_4$-$Na(Yb,Er)F_4$, $Na(Y,Yb)F_4$-$Na(Yb,Er)F_4$, $NaYbF_4$-$NaErF_4$, $Na(Y,Yb)F_4$-$NaErF_4$ and $Na(Y,Yb,Er)F_4$-$NaYF_4$ were synthesized with the co-precipitation method [13] to improve the up-conversion luminescence efficiency by enhancing the energy transfer from ytterbium to erbium. Also a homogeneous $Na(Y,Yb,Er)F_4$ nanomaterial was prepared as a reference. The materials' purity was studied with FT-IR spectroscopy. The crystal structures were characterized with X-ray powder diffraction (XPD) and the crystallite sizes were calculated with the Scherrer formula [14] from the diffraction data. The up-conversion luminescence and red luminescence decay were studied with NIR laser excitation at 970 nm.

Experimental

Materials preparation

The nanocrystalline $NaRF_4$-$NaR'F_4$ materials were prepared with the co-precipitation method [13]. In a typical procedure, the $NaRF_4$ core was prepared by dissolving first 2.1 g of NaF in 60 cm^3 of deionized water. Excess NaF was used to ensure the complete reaction. Another solution was prepared by mixing together selected aqueous solutions of YCl_3 (16), $YbCl_3$ (3.4), and/or $ErCl_3$ (0.6 cm^3). The concentration of these solutions was 0.2 $moldm^{-3}$. The volume of each RCl_3 solution was always constant in the core-shell nanomaterials. The chloride solution was poured quickly into the NaF solution, and the mixture was stirred for 1 h at room temperature. The precipitate from the reaction was centrifuged, washed three times with deionized water and once with anhydrous ethanol. The precipitate was then dried under vacuum.

The dried core was mixed into an aqueous solution of NaF (60 cm^3). The selected $R'Cl_3$ solutions (YCl_3 (16), $YbCl_3$ (3.4), and/or $ErCl_3$ (0.6 cm^3)) were poured quickly into the NaF-$NaRF_4$-core solution, and the mixture was stirred for 1 h at room temperature. The precipitate was centrifuged, washed and dried as above.

The nanoparticles were annealed at 600 °C for five hours under a static N_2 + 10% H_2 gas sphere (heating rate: 20 °Cmin^{-1}). After annealing, the materials were cooled down freely to room temperature under the same gas sphere. All the products, $4NaYF_4$-$Na(Yb_{0.85}Er_{0.15})F_4$, $5Na(Y_{0.82}Yb_{0.18})F_4$-$Na(Yb_{0.85}Er_{0.15})F_4$, $6NaYbF_4$-$NaErF_4$, $32Na(Y_{0.82}Yb_{0.18})F_4$-$NaErF_4$ and $Na(Y_{0.80}Yb_{0.17}Er_{0.03})F_4$-$NaYF_4$, presented with the ideal molar ratios of the core and shell, were fine, white powders.

Characterization

The crystal structures and phase purities of the materials were analyzed with X-ray powder diffraction measurements. The patterns were collected at room temperature between 4 and 100° (in 2θ) with a Huber G670 image plate Guinier camera ($CuK_{\alpha1}$ radiation, 1.5406 Å). The data collection time was 30 min.

The FT-IR spectra between 400 and 4,000 cm^{-1} were measured at room temperature with a Mattson Instruments GALAXY 6030 spectrometer. The material was mixed with KBr and then pressed to a transparent disc.

The crystallite sizes of the $NaRF_4$-$NaR'F_4$ materials were estimated from the diffraction data using the Scherrer formula (Eq. 1) [14]. In this equation, d is the mean crystallite size (m), λ the X-ray wavelength (m), β (rad) the full width at half maximum (FWHM) of the [111] reflection (2θ: 28.2°) for the cubic and the [101] reflection (2θ: 30.9°) for the hexagonal phase and θ (°) half of the Bragg´s angle (2θ). The reflection broadening due to the diffractometer was eliminated from the $β_s$ value by using a microcrystal-line reference ($β_r$) (Eq. 2). A commercial, microcrystalline $NaYF_4$:Yb^{3+},Er^{3+} (PTIR 550/F, Phosphor Technology Ltd, Stevenage, England) was used as a reference.

$$d = \frac{0.9\lambda}{\beta\cos\theta} \tag{1}$$

$$\beta^2 = \beta_s^2 - \beta_r^2 \tag{2}$$

The up-conversion luminescence spectra of the nano-materials were measured at room temperature with an Ocean Optics PC2000-CCD optical fiber spectrometer. The NIR excitation (970 nm) source was a HTOE FLMM-0980-711-1300 m fiber-coupled NIR laser diode (radiation power 670 mW). There was a longpass filter (850 nm, Edmunds RG850) between the laser and the sample and a shortpass filter (850 nm, Edmunds 46386) between the sample and spectrometer. The shortpass filter was used to exclude the exciting radiation from the detector. The material was packed inside a capillary tube as evenly as possible. The spectral response of the spectrometer was calibrated with an Ocean Optics LS-1-CAL-INT calibration source.

The red up-conversion luminescence decays were measured with the same excitation source. An interference filter (Thorlabs FB650-10) was used to select the red emission (650 nm) of the sample. The sample emission was detected with a photomultiplier tube (Hamamatsu R1464). The excitation pulse duration was 40 ms. After each pulse there was a 60 ms delay before the next pulse. One measurement consisted of 2,000 pulse-delay cycles.

Results and discussion

Crystal structure

The XPD patterns revealed the presence of both the cubic (Fm$\overline{3}$m (#225), Z: 2) [15] and hexagonal (P$\overline{6}$ (#174), Z: 1.5) [15] NaRF$_4$ phases (Fig. 1). In the cubic structure, the Na and Y atoms are randomly distributed in the single cation site with statistical 50 % occupancies for both atoms [16, 17]. In the hexagonal structure there are three different types of cation sites. The hexagonal phase is thermodynamically more stable and the cubic to hexagonal phase transition is of the disorder-to-order type [16].

The structure of the homogeneous Na(Y,Yb,Er)F$_4$ materials was hexagonal, whereas in the NaRF$_4$-NaR'F$_4$ materials there were both cubic and hexagonal phases present (Fig. 1). The molar ratio of the core and shell of the NaRF$_4$-NaR'F$_4$ materials varied due to the different ratios of the materials used for the core and shell. In the case of the 4NaYF$_4$-Na(Yb,Er)F$_4$ and 5Na(Y,Yb)F$_4$-Na(Yb,Er)F$_4$ materials with a relatively high amount of the shell material, the proportion of the hexagonal phase (cubic/hexagonal ratio 1 and 3, respectively) was higher than with the 6NaYbF$_4$-NaErF$_4$ and 32Na(Y,Yb)F$_4$-NaErF$_4$ materials (cubic/hexagonal ratio 8 and 6, respectively) with lower amount of the shell material. According to these results, it can be assumed that the structure of the core is mainly cubic and the shell hexagonal. In other words, the shell layer may prevent the phase transition of the core from cubic to hexagonal during the annealing. In the case of the Na(Y,Yb,Er)F$_4$-NaYF$_4$ material, with large cubic/hexagonal ratio (15), this is not so evident despite of the high amount of the shell material.

The diffraction reflections of the NaYbF$_4$-NaErF$_4$ material were moved towards higher 2θ values compared to the other materials containing yttrium ions (Fig. 1). This is due to the smaller ionic radii of Yb^{3+} (0.985) and Er^{3+} (1.004) compared to that of Y^{3+} (1.019 Å; CN: 8) [18]. The calculated crystallite sizes were approximately 100 and 150 nm for the cubic and hexagonal phases, respectively. The crystallite sizes of the core-shell materials were nearly equal to that for the homogeneous Na(Y,Yb,Er)F$_4$. However, from the present diffraction data, it is difficult to judge whether core-shell structures have been formed or to what extent the core and shell contents have been mixed during the heating.

Materials purity

The metal-fluoride vibrations in the FT-IR spectra (Fig. 2) revealed, in agreement with the XPD data, that there were both cubic and hexagonal phases in the core-shell NaRF$_4$-NaR'F$_4$ materials: a vibration at 550 cm^{-1} was present for the cubic structure. The FT-IR spectra revealed also that the M-F vibrations of the 6NaYbF$_4$-NaErF$_4$ material were moved towards lower energy compared to the other core-shell materials. This is due to the lower M-F stretching frequency with ytterbium (and erbium) than yttrium. The strong OH stretching (3500) and HOH bending (1,550 cm^{-1}) vibrations were mainly due to the water absorbed on the surface of the KBr disc during the preparation. No impurities due to the samples themselves were observed by either XPD or the FT-IR measurements.

Up-conversion luminescence

The up-conversion luminescence was excited by NIR radiation (λ_{exc}: 970 nm). The excitation process for the up-conversion emission of Er^{3+} ions has been well

Fig. 1 X-ray powder diffraction patterns of the NaRF$_4$-NaR'F$_4$ nanomaterials. The cubic reference pattern is for NaYF$_4$ and the hexagonal one Na (Y$_{0.57}$Yb$_{0.39}$Er$_{0.04}$)F$_4$
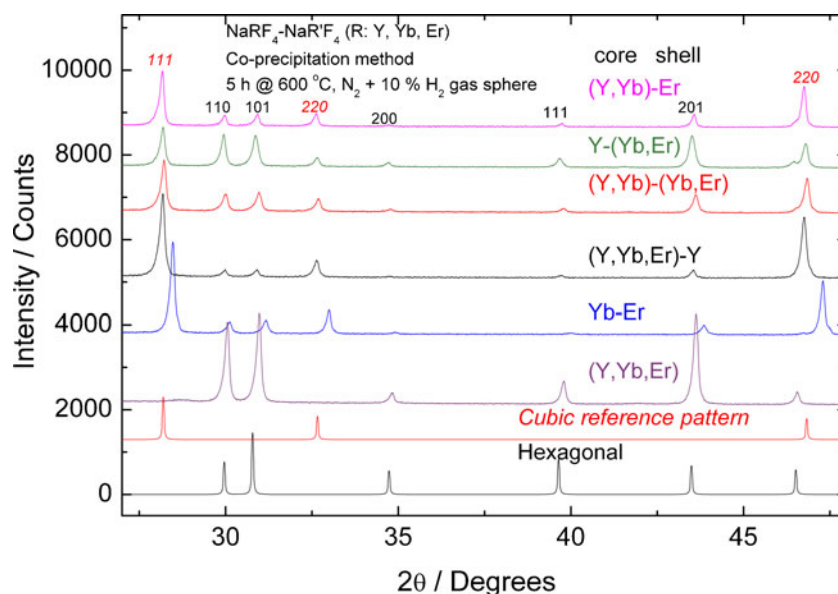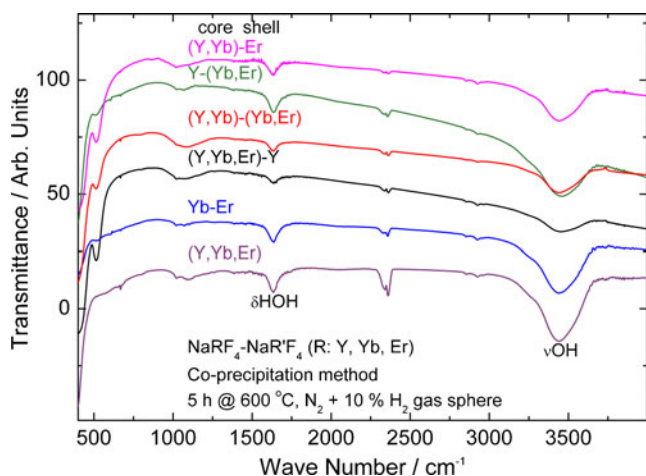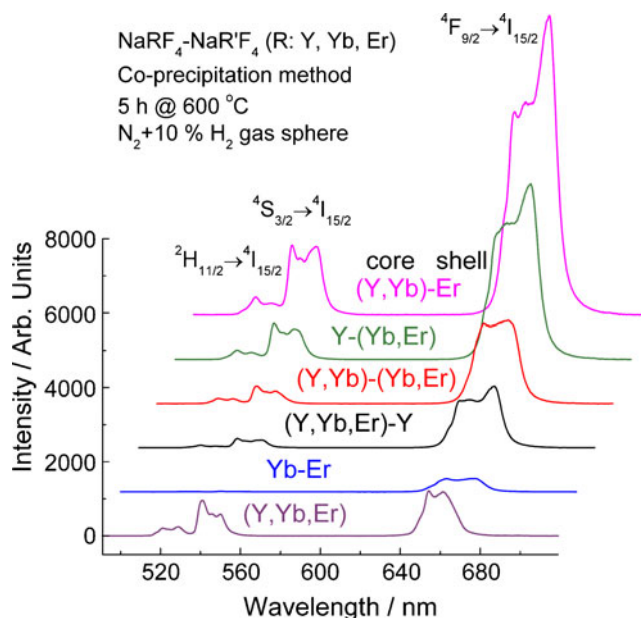
Fig. 2 FT-IR spectra of the NaRF$_4$-NaR′F$_4$ nanomaterials

established in the literature [e.g. 1, 2]. The first photon of infrared radiation excites the Yb^{3+} ion to the $^2F_{5/2}$ level. The excited Yb^{3+} ion may then relax radiatively from this excited level back to the ground level ($^2F_{7/2}$). Alternatively, it can transfer the energy to the Er^{3+} ion. This energy can promote the Er^{3+} ion from the $^4I_{15/2}$ to the $^4I_{11/2}$ level, and if the latter is already populated, a transition from the $^4I_{11/2}$ to the $^4F_{7/2}$ level can occur. The Er^{3+} ion can relax non-radiatively to the $^2H_{11/2}$, $^4S_{3/2}$ or $^4F_{9/2}$ levels. Therefore, green ($^2H_{11/2}$, $^4S_{3/2} \rightarrow {}^4I_{15/2}$, 515–560 nm) and red ($^4F_{9/2} \rightarrow {}^4I_{15/2}$, 640–685 nm) up-conversion emission is obtained from the materials under infrared excitation.

There may be three possible cross-relaxation processes resulting in the quenching of the green luminescence described above. The first process involves the $^2H_{11/2} \rightarrow {}^4I_{13/2}$ relaxation and the $^4I_{9/2} \leftarrow {}^4I_{15/2}$ excitation; the energy being ca. 12,500 cm^{-1}. In the second possible cross-relaxation process, there are coupled the $^2H_{11/2} \rightarrow {}^4I_{9/2}$ relaxation and the $^4I_{13/2} \leftarrow {}^4I_{15/2}$ excitation [19]. The energy difference related to these processes is ca. 6,700 cm^{-1}. It has been claimed that these two cross-relaxation mechanisms competing with the green luminescence are experimentally indistinguishable [20]. The third cross-relaxation process involves the higher excited $^4F_{7/2}$ level of Er^{3+} which relaxes to the red emitting $^4F_{9/2}$ level bypassing the green emitting levels [21]. The energy balance (ca. 5,000 cm^{-1}) is conserved by the excitation of Er^{3+} to the $^4F_{9/2}$ level from the $^4I_{11/2}$ level which is populated due to the NIR laser pumping. Indeed, this process would favor the red emission. The cross-relaxation processes of Er^{3+} are naturally favored by the rather high erbium concentration in the nanomaterials because the erbium ions can locate near each other. This explains the strong red luminescence.

The most intense up-conversion luminescence is obtained from the 32Na(Y,Yb)F$_4$-NaErF$_4$ material (Fig. 3). Also the 4NaYF$_4$-Na(Yb,Er)F$_4$ material produced very efficient luminescence. The shapes of the luminescence spectra of these two materials are similar which reveals that the microdomain favorable for the efficient luminescence around the erbium activator is similar. When comparing these two materials the only difference is the location of the ytterbium sensitizer. It could be thought that it is easier to excite the ytterbium ion when it is in the shell layer and close to the erbium activator ions. However, according to these results, the up-conversion luminescence intensity is more efficient, when the ytterbium ions are in the core. The reason for this might be the inability of the atmospheric impurities (e.g. OH$^-$) to disturb the excitation energy absorption of the ytterbium if it is located in the core. The impurities can also weaken the luminescence of the erbium activator ions, but the effect seems to be rather insignificant considering the efficient up-conversion luminescence of the 32Na(Y,Yb)F$_4$-NaErF$_4$ and 4NaYF$_4$-Na(Yb,Er)F$_4$ materials with the erbium ions in the shell.

The second reason for the efficiency of the 32Na(Y,Yb)F$_4$ -NaErF$_4$ and 4NaYF$_4$-Na(Yb,Er)F$_4$ materials might be the aggregation of the optically active ions. For example, in the case of the 32Na(Y,Yb)F$_4$-NaErF$_4$ material, the ytterbium ions might have been diffused towards the shell layer closer to the erbium ions improving the energy transfer from Yb^{3+} to Er^{3+} while still keeping the local concentration of Er^{3+} low enough to prevent the concentration quenching. For

Fig. 3 Up-conversion luminescence spectra of the NaRF$_4$-NaR′F$_4$ nanomaterials

4NaYF$_4$-Na(Yb,Er)F$_4$ the emission may be weaker due to the too efficient energy transfer in the shell layer resulting in quenching of the emission. Similarly, the weak luminescence of the 6NaYbF$_4$-NaErF$_4$ material might be due to the fact that only a fraction of the Yb^{3+} and Er^{3+} ions, *i.e.* those close to the core/shell boundary are close enough to each other to allow efficient energy transfer (Fig. 3).

Although the hexagonal NaYF$_4$ phase is one of the most efficient lattices for up-conversion luminescence known to date [22, 23], the up-conversion luminescence intensity of the hexagonal, homogeneous Na(Y,Yb,Er)F$_4$ material is rather weak compared to the partially cubic core-shell materials. This is due to the previously mentioned aggregation by diffusion, probably enhanced by the interface between the core and the shell. In the homogeneous material, there is no concentration gradient for the optically active ions and they cannot move towards more favorable places for the up-conversion luminescence. The utilization of core-shell structures can thus be a more efficient way to obtain highly luminescent materials than producing bulk materials which usually need high temperatures [13, 24].

The high I_{red}/I_{green} ratio of the 6NaYbF$_4$-NaErF$_4$ material may be due to the cross-relaxation processes of the erbium ions (Fig. 4). These are enhanced by the high Er^{3+} concentration in the shell layer, which improves the probability of the cross-relaxation processes and increases the red luminescence intensity as well as decreases the green one [19, 21].

The lowest I_{red}/I_{green} ratio was observed with the homogeneous Na(Y,Yb,Er)F$_4$ material, where the red and green luminescence intensities are almost equal (Fig. 4). This is probably due to the lack of the cross-relaxation processes, which, in turn, is caused by the erbium ions located evenly in the NaYF$_4$ host lattice without forming Er^{3+} clusters. Finally, the observed sensitivity of the emission properties to the core-shell composition can be taken as a clear indication of the fact that the materials studied, indeed, possess a core-shell structure.

Up-conversion luminescence decay

The red up-conversion luminescence decay curves (Fig. 5) revealed that the luminescence feeding process is very slow. The saturation point is achieved not until the excitation of 40 ms. The slowest feeding process was observed with the Na(Y,Yb,Er)F$_4$-NaYF$_4$ material. This is due to the weak excitation energy absorption of the ytterbium sensitizer ions located in the core covered by a thick NaYF$_4$ layer. The energy migration in the Yb^{3+}-Yb^{3+} sublattice may slow down the feeding process, as well.

Also in the 32Na(Y,Yb)F$_4$-NaErF$_4$ material the ytterbium sensitizers locate only in the core. However, the feeding process is faster compared to the Na(Y,Yb,Er)F$_4$-NaYF$_4$ material. This is due to the thinner shell layer and the diffusion of the ytterbium ions towards the shell of the first mentioned material which makes the energy absorption easier.

The fastest feeding process was observed with the 6NaYbF$_4$-NaErF$_4$ material (Fig. 5). This is due to the fact that only the energy transferred towards the core-shell interface, *i.e. via* short routes, can reach the Er^{3+} ions. Also the up-conversion luminescence is rather weak since only very few isolated Yb^{3+} and Er^{3+} ions (or Yb^{3+}-Er^{3+} pairs) contribute to the up-conversion luminescence.

The long-duration part of the Er^{3+} decays extends beyond 20 ms for the different NaRF$_4$-NaR′F$_4$ materials (Fig. 5). The relatively intense afterglow indicates that the energy is temporarily stored in traps formed in the material, *e.g.* cation vacancies formed due to the possible excess of R^{3+} ions in the lattice [25]. This afterglow can be called "persistent up-conversion". The persistent up-conversion luminescence has been observed also in the ZrO$_2$:Yb^{3+},Er^{3+} materials [26].

Fig. 4 Red-to-green up-conversion luminescence intensity ratios of the NaRF$_4$-NaR′F$_4$ nanomaterials
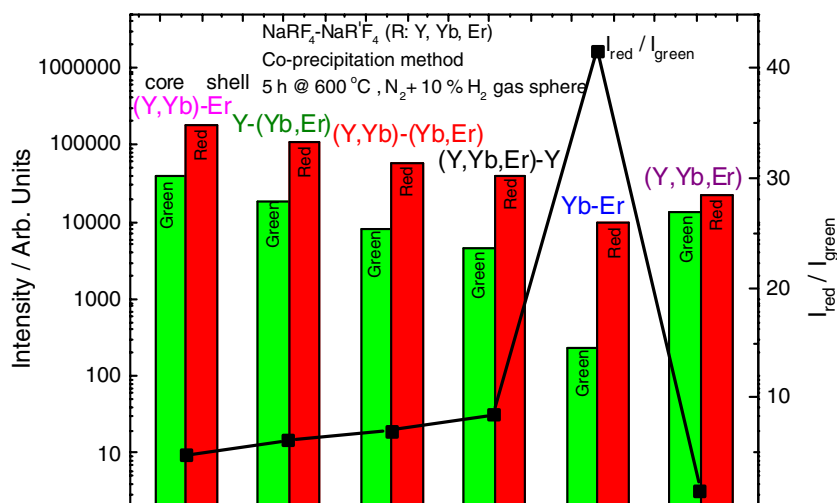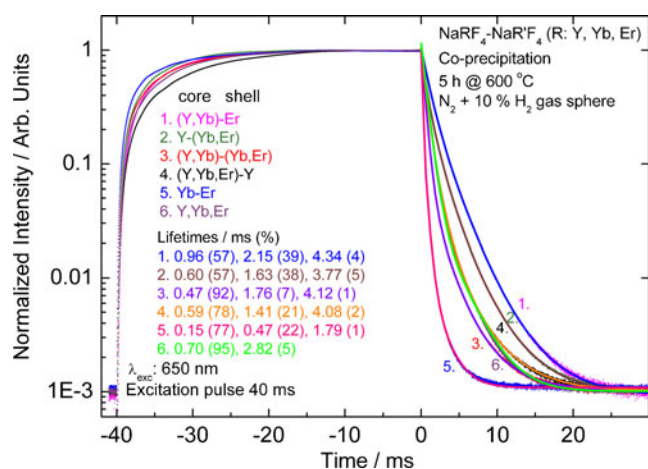
Fig. 5 Red luminescence decays of the $NaRF_4$-$NaR'F_4$ nanomaterials

Conclusions

The $NaRF_4$-$NaR'F_4$ core-shell nanomaterials (R: Y, Yb, Er) were synthesized successfully. The structures of the materials were a mixture of both the cubic and hexagonal phases whereas the homogeneous $Na(Y,Yb,Er)F_4$ material was pure hexagonal. According to the X-ray powder diffraction patterns of the core-shell materials, it can be assumed that the structure of the core is mainly cubic and the shell hexagonal. In other words, the shell layer may prevent the phase transition of the core from cubic to hexagonal during the annealing. The metal-fluoride vibration at 550 cm^{-1} observed in the FT-IR spectra was due to the cubic phase in the $NaRF_4$-$NaR'F_4$ material.

The most intense luminescence is obtained from the $32Na(Y,Yb)F_4$-$NaErF_4$ and $4NaYF_4$-$Na(Yb,Er)F_4$ materials due to the microdomain favorable for the efficient luminescence around the erbium activator. Another reason for the efficient luminescence of these materials might be the aggregation of the dopants improving the energy transfer from Yb^{3+} to Er^{3+}.

The high I_{red}/I_{green} ratio of the $6NaYbF_4$-$NaErF_4$ material might be due to the cross-relaxation processes of the erbium ion clusters. These clusters improved the probability of the cross-relaxation processes, which increased the red luminescence and decreased the green one. The lowest I_{red}/I_{green} ratio was observed with the homogeneous $Na(Y,Yb,Er)F_4$ material due to the lack of the cross-relaxation processes, caused by the erbium ions located evenly in the $NaYF_4$ host lattice without forming the Er^{3+} clusters.

The slowest red luminescence feeding process was observed with the $Na(Y,Yb,Er)F_4$-$NaYF_4$ material due to the weak excitation energy absorption of the ytterbium sensitizer ions locating in the core and covered by a thick $NaYF_4$ layer. The energy migration in the Yb^{3+}-Yb^{3+} sublattice may slow down the feeding process, as well. The fastest feeding process was observed with the $6NaYbF_4$-$NaErF_4$ material. The relatively intense afterglow indicates that the energy is temporarily stored in the defects formed in the material during the synthesis.

References

1. Auzel F (2004) Upconversion and anti-Stokes processes with f and d ions in solids. Chem Rev 104:139–173
2. Mita Y (1999) In: Shionoya S, Yen WM (eds) Phosphor handbook. CRC Press, Boca Raton, pp 643–650
3. Mai H-X, Zhang Y-W, Sun L-D, Yan CH (2007) Highly efficient multicolor upconversion emissions and their mechanisms of monodisperse $NaYF_4$:Yb, Er core and core/shell-structured nanocrystals. J Phys Chem C 111:13721–13729
4. Zhang Q, Zhang Q-M (2009) Synthesis and photoluminescence properties of α-$NaYF_4$:Nd/α-$NaYF_4$ core/shell nanostructure with enhanced near infrared (NIR) emission. Mater Lett 63:376–378
5. Yi G-S, Chow G-M (2007) Water-soluble $NaYF_4$:Yb, Er(Tm)/ $NaYF_4$/polymer core/shell/shell nanoparticles with significant enhancement of up-conversion fluorescence. Chem Mater 19:341–343
6. Park OK, Kang YS (2005) Preparation and characterization of silica-coated TiO_2 nanoparticle. Colloids Surf A 257–258:261–265
7. Ohmori M, Matijević E (1993) Preparation and properties of uniform coated inorganic colloidal particles: 8. Silica on iron. J Colloid Interface Sci 160:288–292
8. Sivakumar S, Diamente PR, Van Veggel FCJM (2006) Silica-coated Ln^{3+}-doped LaF_3 nanoparticles as robust down-and upconverting biolabels. Chem Eur J 12:5878–5884
9. Li Y, Liu ECY, Pickett N, Skabara PJ, Cummins SS, Ryley S, Sutherland AJ, O'Brien P (2005) Synthesis and characterization of CdS quantum dots in polystyrene microbeads. J Mater Chem 15:1238–1243
10. Kömpe K, Borchert H, Storz J, Lobo A, Adam S, Müller T, Haase M (2003) Green-emitting $CePO_4$:Tb/$LaPO_4$ core-shell nanoparticles with 70% photoluminescence quantum yield. Angew Chem Int Ed 42:5513–5516
11. Xie MY, Yu L, He H, Yu XF (2009) Synthesis of highly fluorescent LaF_3:Ln^{3+}/LaF_3 core/shell nanocrystals by a surfactant-free aqueous solution route. J Solid State Chem 182:597–601
12. Wang Y, Tu L, Zhao J, Sun Y, Kong X, Zhang H (2009) Upconversion luminescence of β-$NaYF_4$:Yb^{3+}, Er^{3+}@β-$NaYF_4$ core/shell nanoparticles: excitation power density and surface dependence. J Phys Chem C 113:7164–7169
13. Yi G, Lu H, Zhao S, Ge Y, Yang W, Chen D, Guo L-H (2004) Synthesis, characterization, and biological application of size-controlled nanocrystalline $NaYF_4$:Yb, Er infrared-to-visible up-conversion phosphors. Nano Lett 4:2191–2196
14. Klug HP, Alexander LE (1959) X-Ray powder diffraction procedures. Wiley, New York, p 491

15. PCPDFWIN v. 1.30, Powder Diffraction File, International Centre for Diffraction Data, entries 06-0342 (cubic NaYF$_4$) and 28-1192 (hexagonal Na(Y$_{0.57}$Yb$_{0.39}$Er$_{0.04}$)F$_4$)

16. Liang X, Wang X, Zhuang J, Peng Q, Li Y (2007) Synthesis of NaYF$_4$ nanocrystals with predictable phase and shape. Adv Funct Mater 17:2757–2765

17. Zhao J, Sun Y, Kong X, Tian L, Wang Y, Tu L, Zhao J, Zhang H (2008) Controlled synthesis, formation mechanism, and great enhancement of red upconversion luminescence of NaYF$_4$:Yb^{3+}, Er^{3+} nanocrystals/submicroplates at low doping level. J Phys Chem B 112:15666–15672

18. Shannon RD (1976) Revised effective ionic radii and systematic studies of interatomic distances in halides and chalcogenides. Acta Cryst A 32:751–767

19. Patra A, Friend CS, Kapoor R, Prasad PN (2003) Effect of crystal nature on upconversion luminescence in Er^{3+}:ZrO$_2$ nanocrystals. Appl Phys Lett 83:284–286

20. Campbell M, Flint CD (1998) Back transfer in the ^{4}S$_{3/2}$ state of Cs$_2$NaEr$_x$Y$_{1-x}$Cl$_6$: extension of the shell model. Spectrochim Acta Part A 54:1583–1591

21. Vetrone F, Boyer JC, Capobianco JA, Speghini A, Bettinelli M (2003) Concentration-dependent near-infrared to visible upconversion in nanocrystalline and bulk Y$_2$O$_3$:Er^{3+}. Chem Mater 15:2737–2743

22. Sommerdijk JL (1973) Influence of host lattice on the infrared-excited visible luminescence in Yb^{3+}, Er^{3+} -doped fluorides. J Lumin 6:61–67

23. Bril A, Sommerdijk JL, De Jager AW (1975) On the efficiency of Yb^{3+}-Er^{3+} activated up-conversion phosphors. J Electrochem Soc 122:660–663

24. Wei Y, Lu F, Zhang X, Chen D (2006) Synthesis of oil-dispersible hexagonal-phase and hexagonal-shaped NaYF$_4$:Yb, Er nanoplates. Chem Mater 18:5733–5737

25. Krämer KW, Biner D, Frei, G, Güdel HU, Hehlen M, Lüthi SR (2004) Hexagonal sodium yttrium fluoride based green and blue emitting upconversion phosphors. Chem Mater 16:1244–1251

26. Hyppänen I, Hölsä J, Kankare J, Lastusaari M, Pihlgren L (2007) Upconversion properties of nanocrystalline ZrO$_2$:Yb^{3+},Er^{3+} phosphors. J Nanomater Article ID 16391